Dilute Potts model in two dimensions

Xiaofeng Qian,[1] Youjin Deng,[2,*] and Henk W. J. Blöte[1,2]
[1]*Lorentz Institute, Leiden University, P. O. Box 9506, 2300 RA Leiden, The Netherlands*
[2]*Faculty of Applied Sciences, Delft University of Technology, P. O. Box 5046, 2600 GA Delft, The Netherlands*
(Received 21 July 2005; revised manuscript received 26 September 2005; published 29 November 2005)

We study the two-dimensional dilute q-state Potts model by means of transfer-matrix and Monte Carlo methods. Using the random-cluster representation, we include noninteger values of q. We locate phase transitions in the three-dimensional parameter space of q, the Potts coupling $K \geqslant 0$, and the chemical potential of the vacancies. The critical plane is found to contain a line of fixed points that divides into a critical branch and a tricritical one, just as predicted by the renormalization scenario formulated by Nienhuis *et al.* for the dilute Potts model. The universal properties along the line of fixed points agree with the theoretical predictions. We also determine the density of the vacancies along these branches. For $q=2-\sqrt{2}$ we obtain the phase diagram in a three-dimensional parameter space that also includes a coupling $V \geqslant 0$ between the vacancies. For $q=2$, the latter space contains the Blume-Capel model as a special case. We include a determination of the tricritical point of this model, as well as an analysis of percolation clusters constructed on tricritical Potts configurations for noninteger q. This percolation study is based on Monte Carlo algorithms that include local updates flipping between Potts sites and vacancies. The bond updates are performed locally for $q<1$ and by means of a cluster algorithm for $q>1$. The updates for $q>1$ use a number of operations per site independent of the system size.

DOI: 10.1103/PhysRevE.72.056132 PACS number(s): 05.50.+q, 05.10.Ln, 64.60.Fr, 75.10.Hk

I. INTRODUCTION

The renormalization scenario for the dilute q-state Potts model, as formulated by Nienhuis *et al.* [1] has been remarkably successful in reproducing known properties of the two-dimensional Potts model such as the qualitative q dependence of the temperature exponent, the first-order character of the phase transition [2] when q exceeds a certain threshold, and the existence of a branch of tricritical points that merges with the critical manifold at this threshold. The renormalization equations as, e.g., analyzed by Nauenberg and Scalapino [3] and others [4,5] even allow the accurate reproduction of subtle details in the mathematical form of free-energy singularity, including the energy discontinuity as a function of q for $q>4$, which was exactly calculated by Baxter [2]. While this strongly suggests that the renormalization description of Ref. [1] is true in a fundamental sense, this approach is not very suitable to obtain quantitative information on the phase diagram. For instance, the renormalization equations of [1] locate the threshold value of q near $q=4.73$ instead of at the exact value [2] $q=4$.

The present work aims to obtain some quantitative information about the model described by the three temperature-like parameters of Ref. [1]. In addition to the Potts coupling K and the chemical potential D of the vacancies, the model also includes a vacancy-vacancy coupling V. It is thus described by the Hamiltonian

$$\mathcal{H}/k_{\mathrm{B}}T = -K\sum_{\langle ij\rangle}\delta_{\sigma_i\sigma_j}(1-\delta_{\sigma_i 0}) - V\sum_{\langle ij\rangle}\delta_{\sigma_i 0}\delta_{\sigma_j 0} - D\sum_k \delta_{\sigma_k 0}, \tag{1}$$

where the variables σ_i carry indices that refer to the sites of a square lattice. They can assume values $\sigma_i=0,1,\ldots,q$, where $\sigma_i=0$ stands for a vacancy and $\sigma_i\neq 0$ for one of the Potts states. The sums on $\langle ij\rangle$ run over all pairs of nearest neighbors. While Nienhuis *et al.* defined their model on the triangular lattice, we do not expect qualitative differences with respect to the model on the square lattice.

The partition sum of the model described by Eq. (1) is

$$Z_\sigma = \left(\prod_{i=1}^{N}\sum_{\sigma_i=0}^{q}\right)\left(\prod_{\langle ij\rangle}\exp[K\delta_{\sigma_i\sigma_j}(1-\delta_{\sigma_i 0})]\exp(V\delta_{\sigma_i 0}\delta_{\sigma_j 0})\right) \times\left(\prod_k \exp(D\delta_{\sigma_k 0})\right). \tag{2}$$

It is convenient to specify the vacancies by a separate variable τ_i that assumes the values 0 (for vacancies) or 1. This leads to

$$Z_\sigma = \left(\prod_{i=1}^{N}\sum_{\tau_i=0}^{1}\sum_{\sigma_i=\tau_i}^{q\tau_i}\right)\left(\prod_{\langle ij\rangle}\exp(K\delta_{\sigma_i\sigma_j}\tau_i)\exp(V\delta_{\tau_i 0}\delta_{\tau_j 0})\right) \times\left(\prod_k \exp(D\delta_{\tau_k 0})\right). \tag{3}$$

For the purpose of the mapping on the random-cluster model, we rewrite $\exp(K\delta_{\sigma_i\sigma_j}\tau_i)=\sum_{b_{ij}=0}^{\tau_i\tau_j}(u\delta_{\sigma_i\sigma_j})^{b_{ij}}$ where $u \equiv e^K-1$ is the temperaturelike parameter, and with the convention $0^0=1$. Substitution in Eq. (3) yields

*Present address: Department of Physics, New York University, 4 Washington Place, New York, NY 10003, USA.

$$Z_\sigma = \left(\prod_{i=1}^{N} \sum_{\tau_i=0}^{1} \right) \left(\prod_{i=1}^{N} \sum_{\sigma_i=\tau_i}^{q\tau_i} \right) \left(\prod_{\langle ij \rangle} \sum_{b_{ij}=0}^{\tau_i \tau_j} (u \delta_{\sigma_i \sigma_j})^{b_{ij}} \exp(V \delta_{\tau_i 0} \delta_{\tau_j 0}) \right) \times \left(\prod_k \exp(D \delta_{\tau_k 0}) \right). \quad (4)$$

Nonzero bond variables $b_{ij}=1$ may occur only on lattice edges connecting equal, nonzero Potts variables. Also in the presence of vacancies we can execute the summation on the Potts variables $\sigma_i=1,\ldots,q$, i.e., perform the Kasteleyn-Fortuin mapping [6]. While Kasteleyn and Fortuin did not include vacancies, they formulated this mapping for a general lattice, so that it can be applied directly to each term in the sum on the vacancy configurations as expressed by the τ_i. The sum on the Potts variables yields a factor q for each cluster of sites connected by nonzero bonds. This yields the random-cluster representation of the Potts model with vacancies:

$$Z_\sigma = Z_b \equiv \left(\prod_{i=1}^{N} \sum_{\tau_i=0}^{1} \right) \left(\prod_{\langle ij \rangle} \sum_{b_{ij}=0}^{\tau_i \tau_j} \right) u^{N_b} q^{N_c} \exp(V N_{vv}) \exp(D N_v), \quad (5)$$

where $N_b \equiv \Sigma b_{ij}$ denotes the number of nonzero bonds. These bonds divide the lattice into N_c clusters or components, N_v denotes the number of vacancies, and N_{vv} the number of nearest-neighbor vacancy pairs as specified by the site variables τ_i.

Although Eqs. (1) and (2) are meaningful only when the number of states is an integer $q \geqslant 1$, Eq. (5) is well defined also for noninteger q. It has played a useful role (together with its simplified version that excludes vacancies) in mappings on the eight-vertex model and on the Coulomb gas, so that exact critical exponents could be obtained [7]. They can be expressed in the Coulomb gas coupling constant g which depends on q by

$$q = 2 + 2 \cos \frac{g\pi}{2} \quad (6)$$

with $2 \leqslant g \leqslant 4$ for the critical and $4 < g \leqslant 6$ for the tricritical Potts model. The temperature dimension followed as

$$X_t = \frac{6}{g} - 1 \quad (7)$$

and the magnetic dimension as

$$X_h = 1 - \frac{g}{8} - \frac{3}{2g}. \quad (8)$$

These dimensions were also exactly derived in the theory of conformal invariance [8]. In this context one characterizes universality classes by a number m related to the Coulomb gas coupling g by $m=g/(4-g)$ for the critical branch ($g \leqslant 4$) and by $m=4/(g-4)$ for the tricritical branch ($g>4$). The theory predicts that there exists a set of scaling dimensions, associated with scalar observables. Some of these dimensions can be labeled by two integers p and q, and are determined by the Kac formula as

$$X_{p,q} = \frac{[p(m+1) - qm)]^2 - 1}{2m(m+1)}. \quad (9)$$

For the critical branch we may identify the ith temperature dimension with $X_{i+1,1}$, and for the tricritical branch with $X_{1,i+1}$. The most relevant magnetic dimension is $X_{(m+1)/2,(m+1)/2}$ for the critical Potts model and $X_{m/2,m/2}$ for the tricritical Potts model.

While considerable exact information is thus available, there remain some problems that have thus far escaped exact analysis. We mention the backbone exponents [9–11], surface critical phenomena [12–14], and percolation properties of random clusters [15]. These problems can in principle be solved by numerical work. For the critical Potts model, one can simply Monte Carlo simulate the model without vacancies. But for $q \approx 4$, strong corrections to scaling occur due to the subleading temperature field, which becomes marginal at $q=4$ and thus generates logarithmic corrections. It is therefore desirable to determine the locus of fixed points, naturally in a truncated parameter space. In a two-dimensional space, the two leading temperature fields thus vanish at this locus. For the critical branch, this would mean that the leading corrections to scaling are suppressed, so that accurate numerical investigations become feasible. For $q<4$ one expects to find, in addition to the critical fixed point, a second fixed point corresponding with the Potts tricritical point, which may also be of some use for numerical work. Here we remark that, for some purposes, an exact result of Nienhuis [16] may offer a good alternative for numerical work on tricritical Potts models. Another research subject that may benefit from accurate knowledge of critical points of models with vacancies concerns the finite-size scaling behavior of models with a constraint. The scaling theory of such models in the thermodynamic limit is described by the Fisher renormalization theory [17]. These phenomena can be investigated numerically in systems whose number of vacancies is conserved by the constraint. The geometric cluster algorithm [18] provides a very suitable tool for such investigations, because it not only conserves the number of vacancies, but also reduces critical slowing down. However, its useful applications are restricted to integer values of q.

The present work aims to provide accurate information on the location of the fixed points and the phase diagram. Most of this program is realized by means of transfer-matrix calculations which are explained in Sec. II, which also contains a short description of the Monte Carlo algorithms employed in this work. In Sec. III we present results for the phase diagram in the (q,K,D) parameter space, in particular the line of fixed points consisting of a critical branch and a tricritical one. This part is restricted to the case $V=0$. For one special value $q=2-\sqrt{2}$ we determine the phase diagram in the three-dimensional space (K,V,D). The results, which are probably generically true [1] for $q<3$ Potts models, are reported in Sec. IV. Section V presents various results including a critical and a tricritical point of the Blume-Capel model, and the location and exponents of the percolation threshold of tricritical Potts clusters for several values of q. Finally, our conclusions are listed in Sec. VI.

II. ALGORITHMS

A. Transfer-matrix technique

We summarize the calculations performed for the continuous-q model defined by Eq. (5). Additional analyses were performed using integer spin representations which are already adequately described in the literature [19] and do not need further explanation. We define the random-cluster model on a lattice on the surface of a cylinder, with one set of nearest-neighbor edges parallel to the transfer direction, i.e., the axis of the cylinder. The cylinder has a length of n lattice units, and has an open end at the nth layer of L sites. The construction of a transfer matrix requires a "coding" of the relevant degrees of freedom at the free end of the cylinder. These degrees of freedom include the positions of the vacancies, and how the remaining sites are connected by the random-cluster bonds. This information is called "connectivity." The somewhat elaborate task of coding these connectivities is described in Appendix A, and the actual definition of the transfer matrix in Appendix B, which is used to build an algorithm that can multiply a vector $\vec{v}$ by the transfer matrix $\mathbf{T}$:

$$\vec{v}' = \mathbf{T} \cdot \vec{v}. \tag{10}$$

It is not necessary to store the full matrix $\mathbf{T}$. The availability of a numerical procedure that executes this multiplication is sufficient for the calculation of a few of the largest eigenvalues. The power method, or direct iteration, would lead to the desired result but the projection of the transfer matrix on a relatively low-dimensional Hessenberg matrix, which was explained in detail in Ref. [20], leads to much faster convergence. As explained in Appendix B, the transfer matrix can be viewed as consisting of two independent sectors, a "nonmagnetic" and a "magnetic" sector. Three different eigenvalues were calculated, namely, the largest eigenvalues in both sectors, and a second eigenvalue in the nonmagnetic sector.

Calculations with finite sizes up to $L=12$ (for the determination of the critical and tricritical points) or $L=13$ (for the determination of the vacancy densities) were performed. The size of the matrix $\mathbf{T}$ is $19\,181\,100 \times 19\,181\,100$ for the latter system size.

1. Calculation of the scaling dimensions

The Potts magnetic correlation function along the coordinate r in the length direction of the cylinder is defined as

$$g_h(r) = \frac{\langle q\delta_{\sigma_0\sigma_r} - 1\rangle}{q-1}. \tag{11}$$

In the random-cluster representation, this correlation function is equal to the probability that sites 0 and r belong to the same random cluster. At large r, $g_h(r)$ decays exponentially with a characteristic length scale ξ_h that depends on K, D, V, and L:

$$g_h(r) \propto e^{-r/\xi_h(K,V,D,L)}, \tag{12}$$

and can be calculated from the largest two eigenvalues λ_0 and λ_1 of the transfer matrix:

$$\xi_h^{-1}(K,V,D,L) = \ln(\lambda_0/\lambda_1). \tag{13}$$

For the calculation of the eigenvalues, as needed to find ξ_h, we may employ the following properties of the corresponding eigenvectors. Since the partition sum of the random-cluster model can be expressed using only the nonmagnetic connectivities (see Appendix B), it follows that the largest eigenvalue, which determines the free energy, resides in the nonmagnetic sector. Furthermore, the transfer matrix contains a nondiagonal block of zeros that reflects the fact that the multiplication of a vector with only zeros on the magnetic positions again leads to such a vector. Thus, there exist left-hand eigenvectors with nonzero elements only for magnetic connectivities. The one among these with the largest eigenvalue is associated with the magnetic correlation function. The calculation of this eigenvector, and its eigenvalue λ_1, can thus be restricted to the magnetic sector.

Application of a conformal mapping [21] relates ξ_h on the cylinder with the magnetic scaling dimension X_h (equal to one-half of the magnetic correlation function exponent η). At a critical point (e.g., K adjusted to its critical value $K=K_c$ for given D and V) this exponent obeys

$$X_h \simeq X_h(K,V,D,L) \equiv \frac{L}{2\pi\xi_h(K,V,D,L)}. \tag{14}$$

This is asymptotically true for a critical model in the limit of large L. We may thus use it to estimate X_h numerically, and thereby obtain evidence about the universality class of the model. Or, if the universality class, and thus X_h, are considered known, we may solve for K, V, or D in

$$X_h(K,V,D,L) \simeq X_h \tag{15}$$

to determine the critical subspace.

In addition to ξ_h, it is possible to determine a second correlation length ξ_t describing the exponential decay of the energy-energy correlation function. It is associated with a third eigenvalue λ_2 of the transfer matrix with an eigenvector in the nonmagnetic subspace, just like the one with eigenvalue λ_0. The pertinent eigenvalue can be obtained by means of the projection technique described in Ref. [20]. In analogy with the case of the magnetic correlation length we can use the third eigenvalue λ_2 to estimate the temperature scaling dimension X_t as

$$X_t(K,V,D,L) \equiv \frac{L}{2\pi\xi_t(K,V,D,L)}, \tag{16}$$

where $\xi_t^{-1} = \ln(\lambda_0/\lambda_2)$.

2. Calculation of the vacancy density

In the calculation of the vacancy density we have to take into account that the transfer matrix for general q is essentially nonsymmetric. We define a matrix representation of the density with elements $V_{\alpha\beta} \equiv \delta_{\alpha,\beta} n_v(\alpha)/L$ where $n_v(\alpha)$ is the number of vacancies as implicit in the connectivity α. The expectation value of the vacancy density ρ is, in vector notation,

$$\langle \rho \rangle = \frac{\sum_\alpha [\mathbf{T}^{n-k} \cdot \mathbf{V} \cdot \mathbf{T}^k \cdot \vec{v}_0]_\alpha}{\sum_\alpha [\mathbf{T}^n \cdot \vec{v}_0]_\alpha}, \tag{17}$$

where $\vec{v}_0$ is the Boltzmann weight of the first row of the system. For an infinitely long system we may take both k and $n-k$ to infinity. The right-hand eigenvalue problem of the transfer matrix is

$$\mathbf{T} \cdot \mathbf{R} = \mathbf{R} \cdot \mathbf{\Lambda}, \tag{18}$$

where $\mathbf{R}$ is the matrix of right-hand eigenvectors, arranged as columns of $\mathbf{R}$, and $\mathbf{\Lambda}$ is the diagonal matrix containing the eigenvalues of $\mathbf{T}$. In general we can similarly formulate the left-hand eigenvalue problem as

$$\mathbf{L} \cdot \mathbf{T} = \mathbf{\Lambda} \cdot \mathbf{L}, \tag{19}$$

such that the matrix of left-hand eigenvectors $\mathbf{L}$ is the inverse of $\mathbf{R}$. Next we insert the unit matrix $\mathbf{R} \cdot \mathbf{L}$ between all inner products in Eq. (17):

$$\langle \rho \rangle = \frac{\sum_\alpha [\mathbf{R} \cdot \mathbf{\Lambda}^{n-k} \cdot \mathbf{L} \cdot \mathbf{V} \cdot \mathbf{R} \cdot \mathbf{\Lambda}^k \cdot \mathbf{L} \cdot \vec{v}_0]_\alpha}{\sum_\alpha [\mathbf{R} \cdot \mathbf{\Lambda}^n \cdot \mathbf{L} \cdot \vec{v}_0]_\alpha}. \tag{20}$$

Let Λ_{11} be the largest eigenvalue, which is the only one that survives when the powers k and $n-k$ become large. After dividing out Λ_{11}^n, $\Sigma_\alpha R_{\alpha 1}$, and $\Sigma_\alpha L_{1\alpha}(v_0)_\alpha$, Eq. (20) reduces to

$$\langle \rho \rangle = \sum_\alpha L_{1\alpha} V_{\alpha\alpha} R_{\alpha 1}. \tag{21}$$

Thus the determination of ρ requires the determination of both the right- and left-hand leading eigenvectors. This was realized by means of two independent calculations along the lines described in Ref. [20], one employing the sparse-matrix decomposition of $\mathbf{T}$, and the other that of the transpose of $\mathbf{T}$.

B. Monte Carlo technique

1. Local bond update for dilute Potts models with $0 < q < 1$

For noninteger $q < 1$, no cluster algorithm is available and we developed an algorithm employing local updates, with bond updates as well as site updates. The latter may flip Potts sites $\sigma_i > 0$ into vacancies $\sigma_i = 0$ and vice versa, thus generalizing the algorithms of Sweeney [22] and Gliozzi [23]. A complication in this type of algorithm is that the number of components N_c in Eq. (5) can be changed by a local update, which influences the transition probabilities. Since the determination of the change in N_c caused by a local update is an essentially nonlocal task, the Monte Carlo algorithms are quite slow in comparison with the cluster methods available for $q > 1$. Moreover, now also the four surrounding bond variables enter into the probabilities of flips between vacancies and Potts sites which leads to many possibilities and leads to a rather time-consuming programming task when a relatively optimal algorithm is desired.

The transition probabilities are defined such as to satisfy detailed balance on the basis of the weights defined by the random-cluster partition sum Eq. (5). Simulations under the constraint that the density of the vacancies is conserved are realized by excluding updates leading to states with less than N_v or more than $N_v + 1$ vacancies.

2. Cluster algorithm for dilute Potts models with $q > 1$

A cluster Monte Carlo algorithm for the noninteger $q > 1$ random-cluster model without vacancies [24] is already available. It appears to be an efficient tool for the study of noninteger q-state Potts model [25] and was also applied in Ref. [26]. To include vacancies it is convenient to use a formulation of this algorithm based on a cluster decomposition as given in Ref. [25] (but here we use a slightly different notation, with number 0 referring to vacancies and 1 to one of the Potts states). Colors are randomly assigned, such that color 1 is singled out with a probability $1/q$. This procedure remains essentially the same in the presence of vacancies. After defining the subset of the lattice in state 1, we can thus include local Metropolis-like updates that may flip state-1 site variables into vacancies and vice versa. The advantage is that the bond variables disappear from the transition probabilities which thus become simple, and a site update requires only a number of operations independent of the system size. The summary of the Monte Carlo procedure, starting from a configuration specified by the subset in state 0 (the vacancies) and the random-cluster decomposition of the remaining sites, is as follows. (1) Assign color 1 to each cluster with probability $1/q$; (2) apply local updates flipping between color-1 sites and vacancies; (3) form clusters on the type-1 sites, using a bond probability $u/(u+1)$; and (4) erase the color variables. The use of a probability $1/q$ restricts the useful range of the algorithm to $q > 1$.

The method enables the study the critical and tricritical properties of dilute Potts models. For instance, it can be used to determine fractal properties of noninteger q Potts clusters at tricriticality. Simulations conserving the number of vacancies require a modification of step 2: we no longer allow flips between vacancies and color-1 variables. Instead, we propose local configuration changes involving the interchange of two site variables, chosen at two random positions. Only interchanges of vacancies and color-1 sites are accepted, with acceptance probabilities that are subject to the condition of detailed balance.

III. LINE OF FIXED POINTS FOR $V = 0$

A. Solving the equations for the fixed points

The transfer-matrix algorithms defined in Sec. II A enables the numerical calculation of the functions $X_h(K,D,L)$ and $X_t(K,D,L)$ for a range of finite sizes L. The algorithm numerically calculates these functions for given values of K, D, and L. The dependence on the parameters q and V, which are kept constant for the present, is not explicitly shown. We employ this technique to estimate the critical and tricritical fixed points in the $V = 0$ subspace, by simultaneously solving for the two unknown K and D in the two equations

$$X_h(K,D,L) = X_h, \quad X_t(K,D,L) = X_t, \tag{22}$$

in which we substitute the exactly known values of X_h and X_t as a function of q (see Sec. I). However, the results for the

TABLE I. Fixed points of tricritical and critical dilute Potts models. These are extrapolations of finite-size data for systems with sizes up to $L=12$, except for the case $q=2$ which used sizes up to $L=16$. The vacancy densities ρ are based on data for system sizes up to $L=13$. The results for $g<3$ were rejected (see text). Exact data for the $q=1$ tricritical point are included.

q	g	K_f	D_f	Refined D_f	ρ
0.1	2.2021…	0.334 (5)	−1.0 (1)		
0.5	2.4601…	0.596 (4)	−0.46 (3)		
0.8	2.5903…	0.709 (3)	−0.15 (2)		
2.45	3.1444…	1.065 (2)	0.950 (5)	0.94708 (5)	0.0810 (3)
$2+\sqrt{2-\sqrt{3}}$	19/6	1.0783 (5)	1.004 (3)	1.00460 (5)	0.0838 (2)
2.6	3.1939…	1.0936 (5)	1.068 (2)	1.06687 (5)	0.0871 (1)
2.8	3.2619…	1.1313 (2)	1.2222 (4)	1.22171 (5)	0.09579 (2)
3.0	10/3	1.16941 (2)	1.37655 (5)	1.376483 (5)	0.10528 (1)
3.5	3.5398…	1.27104 (2)	1.77785 (4)	1.777891 (5)	0.13496 (1)
3.8	3.7128…	1.34722 (2)	2.06903 (4)	2.069046 (4)	0.16225 (1)
$2+\sqrt{2+\sqrt{2}}$	15/4	1.36261 (2)	2.12689 (4)	2.126922 (4)	0.16839 (1)
3.9	3.7978…	1.38194 (2)	2.19915 (4)	2.19917 (1)	0.176431 (10)
4.0	4	1.45791 (2)	2.47845 (4)	2.47847 (1)	0.21207 (1)
3.9	4.2021…	1.525175 (4)	2.719730 (8)	2.719732 (3)	0.250190 (5)
3.8	4.2871…	1.551010 (3)	2.810900 (6)	2.810902 (2)	0.266885 (5)
3.5	4.4601…	1.599352 (3)	2.979260 (6)	2.979263 (2)	0.30202 (2)
$2+\sqrt{2}$	9/2	1.609715 (5)	3.014962 (10)	3.014971 (3)	0.31031 (2)
3	14/3	1.649903 (5)	3.152149 (10)	3.152152 (2)	0.345766 (10)
$2+\sqrt{2-\sqrt{2}}$	19/4	1.668155 (5)	3.213760 (10)	3.213758 (3)	0.36396 (4)
2.5	4.8391…	1.686350 (5)	3.274720 (10)	3.274720 (3)	0.3838 (1)
2.0	5	1.715733 (1)	3.372204 (2)	3.372205 (3)	0.42020 (10)
1.5	5.1608…	1.740760 (8)	3.454225 (15)	3.454222 (3)	0.4578 (2)
$2-\sqrt{2-\sqrt{2}}$	21/4	1.752746 (8)	3.493180 (15)	3.493172 (3)	0.4793 (2)
1	16/3	$2\ln(1+\sqrt{2})$	$4\ln(1+\sqrt{2})$		1/2
$2-\sqrt{2}$	11/2	1.77927 (4)	3.57851 (8)	3.578504 (3)	0.5430 (5)
$2-\sqrt{3}$	17/3	1.79110 (5)	3.61617 (10)	3.616170 (4)	0.5885 (8)
0.1	5.7978…	1.7971 (1)	3.6352 (2)	3.63516 (2)	0.630 (10)

fixed points do not critically depend on these exact values, since the numerical procedure includes some redundancy as we shall discuss in Sec. III C. The solutions are denoted $K_f(L)$ and $D_f(L)$, where the index f refers to "fixed point." In order to find their finite-size-scaling properties, we express the functions $X_h(K,D,L)$ and $X_t(K,D,L)$ in terms of the two leading temperature fields t_1 and t_2, and another temperature-like field u that is taken to be irrelevant. Expansion of the finite-size scaling functions yields the equations

$$\begin{aligned} X_h(t_1,t_2,u,L) &= X_h + a_h t_1 L^{y_{t_1}} + b_h t_2 L^{y_{t_2}} + u_h L^{y_i} + \cdots, \\ X_t(t_1,t_2,u,L) &= X_t + a_t t_1 L^{y_{t_1}} + b_t t_2 L^{y_{t_2}} + u_t L^{y_i} + \cdots, \end{aligned} \tag{23}$$

where a_h, b_h, u_h, a_t, b_t, and u_t are unknown constants, y_i is an irrelevant exponent (y_{t_3} or the integer −2), and y_{t_1} and y_{t_2} are the two leading temperature exponents. At the simultaneous solution we thus have

$$\begin{aligned} a_h t_1 L^{y_{t_1}} + b_h t_2 L^{y_{t_2}} + u_h L^{y_i} + \cdots = 0, \\ a_t t_1 L^{y_{t_1}} + b_t t_2 L^{y_{t_2}} + u_t L^{y_i} + \cdots = 0. \end{aligned} \tag{24}$$

Elimination of t_1 and solving for t_2 yields

$$t_2 = \frac{(a_t u_h - a_h u_t)}{(a_h b_t - a_t b_h)} L^{y_i - y_{t_2}}. \tag{25}$$

Similarly, we find the solution for t_1 as

$$t_1 = \frac{(b_t u_h - b_h u_t)}{(a_h b_t - a_t b_h)} L^{y_i - y_{t_1}}. \tag{26}$$

The scaling behavior of the numerical solutions $K_f(L)$ and $D_f(L)$ is found by expressing their differences with the asymptotic values K_f and D_f as linear combinations of t_1 and t_2:

$$K_f(L) = K_f + a_0 L^{y_i - y_{t_2}} + a_1 L^{y_i - y_{t_1}} + \cdots \tag{27}$$

and

$$D_f(L) = D_f + b_0 L^{y_i - y_{t_2}} + b_1 L^{y_i - y_{t_1}} + \cdots, \tag{28}$$

where a_j $(j=0,1,\ldots)$ and b_j $(j=0,1,\ldots)$ are unknown constants. Since we know, in principle, the exponents y_{t_1}, y_{t_2}, and y_i (see Sec. I), we can use this knowledge to extrapolate the solutions to obtain K_f and D_f. Two subsequent finite-size results $K_f(L)$ and $K_f(L+1)$ allow one extrapolation by solving for $K_f^{(1)}(L)$ and a_0 in

$$K_f(L') = K_f^{(1)}(L) + a_0 L^{y_i - y_{t_2}} \tag{29}$$

for $L'=L$ and $L+1$. A second iteration step with a free exponent according to the three-point fits described in Ref. [20] then yielded iterated estimates $K_f^{(2)}(L)$ from which we obtain final estimates listed in Table I. The numerical uncertainty margin in these numbers was estimated from the differences between the $K_f^{(2)}(L)$ obtained for the few largest L available. The data for D_f were analyzed similarly. The actual numerical accuracies of the fixed points are better in the direction perpendicular to the line of phase transitions than along this line. For this reason we have solved for D in the equation $X_h(K,D,L)=X_h$, with K fixed at its estimated fixed-point value K_f, except for $g<3$, because of reasons given below. The solutions were again fitted using similar methods as above. The fits yield refined estimates of D that are included in Table I. The latter estimates are likely to lie closer to the line of phase transitions, but not necessarily closer to the fixed point.

The numerical procedure yielded results with a satisfactory finite-size convergence, except for $q \to 0$ on the tricritical branch, where the results become less accurate because the scaling exponents become indistinguishable from those at the first-order transition, and for $q \lesssim 2.5$ on the critical branch, where complications of a different nature arise. First, it has been reported [7,27] that corrections to scaling due to the second temperature field, i.e., governed by the exponent y_{t_2}, disappear in most observables for $q \to 2$. This means that, near $q=2$, the numerical solutions (if any) do not suppress the second temperature field, but instead other effects, possibly analytic corrections with exponent -2 as in the Ising model. Second, for $q<1$, we have $y_{t_2}<-2$ so that the leading corrections to scaling in Eqs. (24) are the analytic ones, and the procedure will again try to suppress these, instead of the second temperature field. Although numerical solutions were obtained for $q<1$, they should not be interpreted as fixed points in the truncated space of the two leading temperature fields t_1 and t_2.

We have also computed the finite-size data for the vacancy density at the estimated fixed points (K_f, D_f), using the procedure outlined in Sec. II A 2. The scaling behavior of ρ follows by differentiation of the free-energy density to D. When we substitute the scaling relation of the free energy, and linearize D in t_1 and t_2, we obtain

$$\rho(L,u) = \rho_0 + a_1 L^{y_{t_1}-2} + a_2 L^{y_{t_2}-2} + \cdots + b_1 L^{y_{t_1}+y_i-2} + \cdots. \tag{30}$$

Fits according to this expression showed no sign of a nonzero amplitude a_1. Indeed the derivative of the scaling function for the free energy with respect to t_1 must vanish, because the energy of $L \times \infty$ self-dual Potts strips does not depend on L [20]. We thus only used exponents $y_{t_2}-2$ and $y_{t_1}+y_i-2$ in the iterated fitting procedure. The extrapolated values of ρ are sensitive to small deviations in the estimated location of the fixed point. For comparison, we have also computed the finite-size data for the vacancy density at the corresponding finite-size solutions of Eqs. (22). The scaling behavior of these finite-size data for ρ now also contains contributions due to the deviations expressed by Eqs. (25) and (26), which may arise from the dependence of ρ_0, a_1, etc., on t_1 and t_2. Which of these contributions dominates depends on the value of g that parametrizes the fixed line. We have applied many fits, using the predicted correction exponents as well as three-point fits that leave the exponent free. Best estimates were obtained by a comparison between these fits, and with the fit of the data obtained at the extrapolated fixed point. The finite-size dependence of the various fits, and the degree of their mutual consistency allowed us to estimate the numerical accuracy of the extrapolated results for the density as included in Table I.

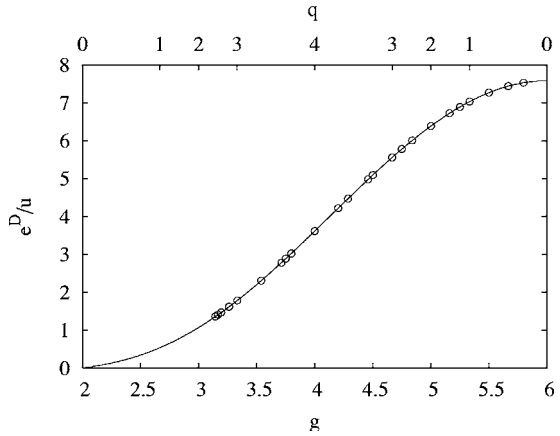

FIG. 1. The line of critical and tricritical fixed points of the dilute Potts model in terms of the ratio e^D/u defined in the text versus the Coulomb gas coupling constant g. These fixed points were obtained in the two-dimensional parameter space (K,D) while V was set equal to zero. The error bars are much smaller than the symbol size. The curve shows the polynomial approximation for e^D/u described in the text. The scale for q is shown above.

B. Polynomial approximations at the line of fixed points

The numerical data presented in Table I appear to behave rather smoothly as a function of the Coulomb gas coupling constant g defined in Sec. I, especially for $g>3$, as shown in Fig. 1. We fitted the quantity $r \equiv e^D/(e^K-1)$ by the expression

$$r(g) = \sum_{j=0}^{5} r_j (g-2)^j, \tag{31}$$

where the coefficients r_j were determined by means of the least-squares criterion. No satisfactory fits, as judged from the residual χ^2, were obtained including all data in Table I, because the data for $g<3$ did not accurately follow the trend

TABLE II. Coefficients of the polynomial describing $r(g)$ along the fixed line as a function of g.

k	r_k	Error
1	0.39815155	0.00250115
2	0.38326777	0.00431988
3	0.44162858	0.00271091
4	−0.16983072	0.00073526
5	0.01472573	0.00007298

of the remaining data, which is understandable on the basis of the relative magnitudes of y_{t_2} and y_i as described in the preceding subsection. A satisfactory fit was however obtained excluding the $g<3$ data. The result for the zeroth-order coefficient $r_0=-0.027$ was slightly negative but not significantly different from 0. Noting that $r\geqslant 0$ for the present model described by Eq. (1), we take this small value as an indication that $r=0$ in the limit $q\downarrow 0$ for the critical fixed point, and thus that the vacancies disappear in this limit. We thus fixed $r_0=0$ and recalculated the coefficients. They are listed in Table II. Figure 1 shows the fit to the numerical results for r as a function of the Coulomb gas coupling constant g.

The fits made use of the exactly known tricritical point for $q=1$, which is equivalent with the Ising model without vacancies. The exact numbers for this point are included in Table I. The addition of this point does not significantly increase the χ^2 residual, which indicates that this point joins smoothly with the numerical data for other values of g.

We have similarly fitted the temperature parameter u as a function of g by the expression

$$u(g)=\sum_{j=1}^{5} u_j(g-2)^j \tag{32}$$

and the density ρ of the vacancies by

$$\rho(g)=\sum_{j=1}^{6} \rho_j(g-2)^j. \tag{33}$$

The number of coefficients was based on the requirement that the residual χ^2 is acceptable. The results are shown in Tables III and IV, respectively. The fitted expression for the density is shown in Fig. 2 as a function of g, together with the numerical data.

TABLE III. Coefficients of the polynomial describing $u(g)$ along the fixed line as a function of g.

k	u_k	Error
1	1.57118750	0.00122031
2	0.11386463	0.00206715
3	−0.01998229	0.00127897
4	−0.01068977	0.00034315
5	0.00093745	0.00003377

TABLE IV. Coefficients of the polynomial describing $\rho(g)$ along the fixed line as a function of g.

k	ρ_k	Error
1	0.01280616	0.00244377
2	0.06353299	0.00594846
3	−0.01922001	0.00564925
4	0.00978198	0.00261807
5	−0.00278903	0.00059244
6	0.00029403	0.00005239

C. Consistency with theory and universality

Our numerical procedure to determine the fixed points relies heavily on the existing results for the magnetic and temperature scaling dimensions, which are not supported by exact analysis for the general case of the model described by Eq. (5). We therefore consider the possibility that the scaling dimensions given by Eqs. (7) and (8) do not apply to the present model. That would lead to an additional constant in Eqs. (23) whose effect is the same as that of a term with an exponent $y_i=0$. Thus, from Eqs. (27) and (28), we would then expect finite-size corrections proportional to $L^{-y_{t_2}}$ in the numerical solutions of Eqs. (22). For the tricritical branch we have $y_{t_2}>0$ so that the solutions for large L still converge to the tricritical fixed point. For Potts criticality we have $y_{t_2}<0$ so that the solutions would fail to converge to the critical fixed point for large L. However, the analysis of the solutions showed satisfactory convergence.

More specifically, the finite-size dependence of the solutions of Eqs. (22) agreed well with the theoretical results for the exponents. This confirms the universality of the Potts model in an extended parameter space.

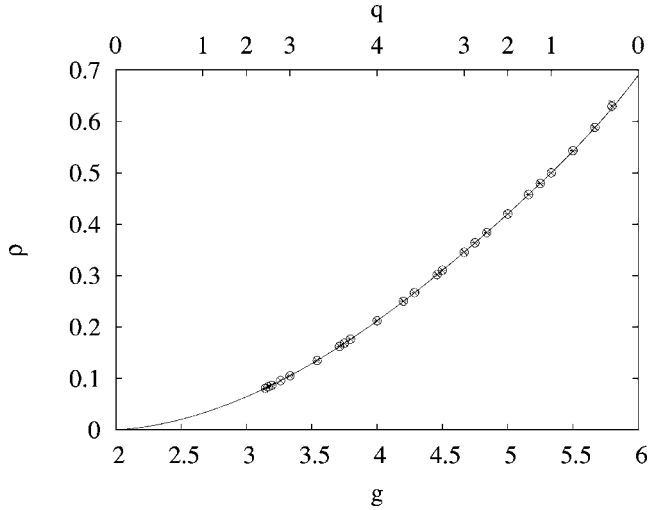

FIG. 2. The vacancy density ρ along the line of fixed points of the dilute Potts model as a function of the Coulomb gas coupling constant g. The error bars are much smaller than the symbol size except for the rightmost data point. The curve shows the polynomial approximation for ρ described in the text. The scale for q is shown above.

As another test, we have analyzed the finite-size dependence of the free energies at the extrapolated fixed points given in Table I. Assuming conformal invariance [8], the conformal anomaly c can be obtained from the reduced free energy $F(L)$ per unit of length of the cylinder, using the formula [28,29]

$$F(L) \simeq Lf_\infty - \frac{\pi c}{6L}, \tag{34}$$

where f_∞ is the reduced bulk free-energy density. This formula applies to the large-L limit. On the other hand, the reduced free energy $F(L)$ per unit of length follows from the largest eigenvalue λ_0 of the transfer matrix as

$$F(L) = -\ln \lambda_0 \tag{35}$$

and can thus be calculated with the procedures outlined in Sec. II A. Since there are two unknowns f_∞ and c in Eq. (34), the substitution of finite-size data for two subsequent system sizes in Eqs. (34) and (35) yields one estimate of the conformal anomaly c. These estimates display a rapid apparent convergence with increasing system sizes, with a finite-size dependence approximately as L^{-2} for most values of q, as deduced from three-point fits (see Ref. [20]). The final estimates of c are shown in Table VII below, together with its theoretical value [28,30]

$$c = 1 - \frac{6}{m(m+1)} \tag{36}$$

in terms of the parameter m defined in Sec. I.

IV. PHASE DIAGRAM FOR $q=2-\sqrt{2}$

We determine the phase diagram in the three-dimensional parameter space (K,D,V) for $K \geqslant 0$ and $V \geqslant 0$, using numerical analysis and some exact arguments. The choice $q=2-\sqrt{2}$, while somewhat arbitrary, was based on the fact that much is already known for the integer values of q, and that the exact results for the critical exponents assume simple fractional values.

A. Equivalences and exact limits

Before presenting the numerical results, we list a few exact results and limiting cases that are helpful to construct the phase diagram. The bond weights offer a handle to identify various phase boundaries and critical points. We consider the following cases.

(1) If both $D+2V \ll 0$ and $D \ll 0$, the vacancies disappear and the Potts critical surface then lies at $K=\ln(1+\sqrt{q})$ [31].

(2) When the Potts coupling vanishes, the dilute Potts model can be mapped on to the Ising model in a field, by interpreting the vacancies as Ising spins of one sign and the remaining site variables as Ising spins of the other sign. The field vanishes for special choices of D and V. For $K=0$ the partition sum Eq. (4) becomes

$$Z_\sigma = \left(\prod_{i=1}^{N} \sum_{\tau_i=0}^{1} \sum_{\sigma_i=\tau_i}^{q\tau_i} \right) \left(\prod_{\langle ij \rangle} \exp(V \delta_{\tau_i 0} \delta_{\tau_j 0}) \right) \left(\prod_{k} \exp(D \delta_{\tau_k 0}) \right). \tag{37}$$

The summand does not explicitly depend on the σ_i, and the sums on the σ_i can thus be executed trivially:

$$Z_\sigma = \left(\prod_{i=1}^{N} \sum_{\tau_i=0}^{1} \right) \left(\prod_{\langle ij \rangle} \exp(V \delta_{\tau_i 0} \delta_{\tau_j 0}) \right) \left(\prod_{k} \exp(D \delta_{\tau_k 0}) q^{\tau_k} \right). \tag{38}$$

After dividing each site weight over the four surrounding bonds, this becomes

$$Z_\sigma = \left(\prod_{i=1}^{N} \sum_{\tau_i=0}^{1} \right) \left(\prod_{\langle ij \rangle} \exp[V \delta_{\tau_i 0} \delta_{\tau_j 0} + D(\delta_{\tau_i 0} + \delta_{\tau_j 0})/4] \times q^{(\tau_i+\tau_j)/4} \right). \tag{39}$$

We compare the bond weights specified by this expression to the zero-field Ising weights $e^{\pm K_I}$ where the sign depends on whether the site variables τ_i and τ_j are equal or not. The black circles represent Potts variables in one of the q states, the black square a Potts different state, and the open circles vacancies:

σ_i	σ_j	dilute Potts	Ising
●	●	$q^{1/2}$	e^{K_I}
●	■	$q^{1/2}$	e^{K_I}
●	○	$q^{1/4} e^{D/4}$	e^{-K_I}
○	○	$e^{V+D/2}$	e^{K_I}

(40)

The dilute Potts model becomes equivalent with the zero-field Ising model when the two types of bond weights are proportional, which holds if

$$K = 0, \quad D + 2V = \ln q. \tag{41}$$

The Ising-like critical point occurs at $K_I=\ln(1+\sqrt{2})/2$ or

$$K = 0, \quad V = 2\ln(1+\sqrt{2}), \quad D = -4\ln(1+\sqrt{2}) + \ln q. \tag{42}$$

The Ising transition is one between a disordered Potts phase and a phase dominated by vacancies. The Ising locus Eqs. (41) contains a first-order line ending in the Ising critical point. It is natural that this coexistence line and critical point extend to nonzero values of K, so that there exists a coexistence plane in the (K,V,D) space, bounded on one side by an Ising critical line.

(3) For $D=0$ and $V=K$, the vacancies become equivalent with the q Potts states, and the model becomes a $(q+1)$-state Potts model. We illustrate this equivalence by listing the bond weights of the dilute q-state Potts model according to Eq. (2) and the bond weights of the $(q+1)$-state Potts model without vacancies. The meaning of the symbols describing the site variables is the same as above:

σ_i	σ_j	dilute Potts	$(q+1)$-state Potts
●	●	e^K	e^K
●	■	1	1
●	○	$e^{D/4}$	1
○	○	$e^{V+D/2}$	e^K

(43)

The phase diagram of the q-state Potts model with vacancies therefore contains a $(q+1)$-state Potts critical point at $D=0$, $V=K=\ln(1+\sqrt{q+1})$.

(4) For $2K=2V+D$ while $D \ll 4K$, the Potts ordered phase and the vacancy-dominated phase balance one another while their interfaces cost much energy. Therefore this condition describes a surface where these two phases coexist.

B. Numerical results

We include the vacancy-vacancy coupling in the transfer-matrix calculation defined in Sec. II A, and locate the Potts critical surface by solving for K at selected values of D, V, and L in

$$X_h(K,V,D,L) = X_h, \tag{44}$$

where we make use of the exact result for X_h quoted in Sec. I. In the vicinity of a critical point, there is only one relevant temperature field, but corrections to scaling may still be generated by irrelevant fields. As a consequence of these corrections, the solution for K will not precisely coincide with a critical point. The effects of an irrelevant scaling field u and a small temperature field t, due to a deviation K from its critical value K_c, are expressed by

$$X_h(K,V,D,L) = X_h + auL^{y_i} + btL^{y_{t_1}} + \cdots, \tag{45}$$

where a and b are unknown constants, and y_{t_1} is the leading temperature exponent. For the present value $q=2-\sqrt{2}$, the corrections are dominated by the exponent $y_i=-2$ which exceeds the second temperature exponent y_{t_2}. The scaling behavior of the numerical solutions $K_c(L)$ is found by expansion of the appropriate scaling function in the leading temperature field, which is in first order proportional to $K-K_c$:

$$K_c(L) = K_c + a_0 L^{y_i - y_{t_1}} + \cdots. \tag{46}$$

The numerical results were found to be consistent with this formula, quite clearly so in parts of the critical surface that are not close to its boundary. Near the boundary, crossover effects become important. We determined critical points K_c for several values of V along six lines of constant D in the interval $-6 \leqslant D \leqslant 4$ as shown in Fig. 3. For most of the critical surface, it proved to be easy to obtain critical points with an accuracy better than 10^{-3} which is sufficient for the graphical presentation of the phase diagram provided in this subsection. Much better accuracies may be obtained if desired; for $D \to -\infty$, where the model reduced to the Potts model without vacancies, we found, using system sizes up to $L=11$, $K_c=0.568\,358$, with an apparent accuracy of less than 10^{-6}. This is consistent with the exact value $K=\ln(1+\sqrt{2-\sqrt{2}})$.

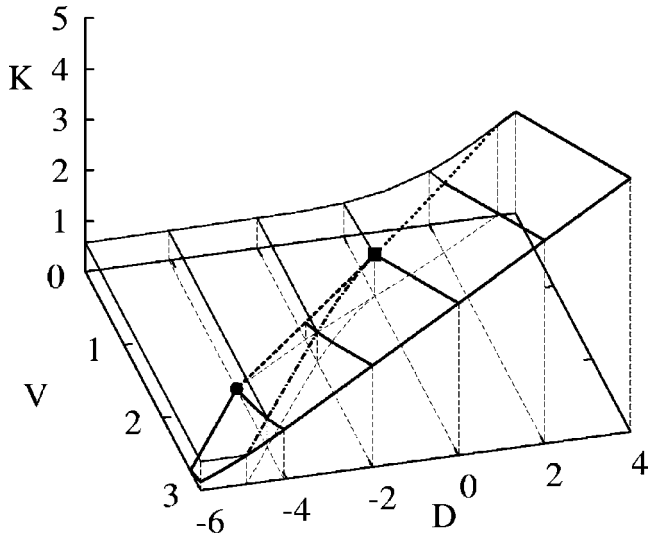

FIG. 3. Phase diagram of the $(2-\sqrt{2})$-state Potts model in the three-dimensional parameter space (V,D,K). The plane of q-state Potts transitions (left-hand side) is outlined by thin solid lines, and that of first-order transitions (right-hand side) by thick solid lines. These lines are shown at constant values $D=-6$, $\ln(58-41\sqrt{2}) \approx -4.06$, -2, 0, 2, and 4. The planes of Potts and first-order transitions merge at a tricritical line (dotted, upper right) and at a critical end line (dash-dotted, lower left). At negative D, the first-order sheet is bounded by an Ising-like critical line on its low-V side (thick dashed, lower left). The intersection of this line with the ground plane $K=0$ is indicated by ●. The critical end line, the Ising line, and the tricritical Potts line meet at the $(q+1)$-state critical point (■). This diagram is constructed on the basis of the arguments presented in Sec. IV A and the numerical results of Sec. IV B.

The plane of these q-state Potts transitions is bounded by a tricritical line for $D>0$. Several points on the tricritical line were solved by means of the numerical technique described in Sec. III A but including V as a parameter. These results indicate that, as expected, the tricritical line does connect to the $(q+1)$-state critical point, as shown in Fig. 3.

We have also used the transfer-matrix technique to numerically investigate the Ising critical point at $K=0$, described in the preceding subsection. Since Potts magnetic correlations are zero, the calculation of X_h yields only divergent results. The calculation of X_t yields results approaching the Ising magnetic dimension 1/8. Indeed, the Ising magnetic correlations, corresponding, e.g., with vacancy-vacancy correlations, are contained in the Potts nonmagnetic sector. We were thus able, by following the behavior of function X_t, to follow the Ising line emerging from the $K=0$ point. We observed that the discontinuous transition between the disordered Potts phase and the vacancy-dominated phase is accompanied by a minimum in the function X_t, with values $<1/8$ and decreasing with L. The Ising critical points can be approximated by requiring that the minimum in the function X_t tends to 1/8. This yields results of a sufficient accuracy for the purpose of constructing Fig. 3.

For $D<0$, the Potts critical surface is not bounded by a tricritical line, but by a critical end line located in the plane of first-order transitions.

V. MISCELLANEOUS RESULTS

A. Blume-Capel model and dilute $q=2$ Potts model

We first describe the relation between the Blume-Capel (BC) model [32], which is the spin-1 Ising model with variable fugacity of the zero spins, and the dilute $q=2$ Potts model. The reduced Hamiltonian of the BC model with nearest-neighbor interactions is

$$\mathcal{H}/k_{\mathrm{B}}T = -K_{\mathrm{BC}}\sum_{\langle ij\rangle} s_i s_j + D_{\mathrm{BC}}\sum_k s_k{}^2, \tag{47}$$

where $s_i=0,\pm 1$, K_{BC} is the nearest-neighbor coupling, and D_{BC} acts as the chemical potential of the vacancies (the sites with $s_i=0$). This Hamiltonian assumes the form of Eq. (1) after the substitution $\sigma_i \equiv (s_i+3s_i^2)/2$. This is most easily shown by comparing the weights per bond for the various values of the site variables. Out of the nine possibilities, only four are independent. Only one-quarter of the site energies $-D_{\mathrm{BC}}s_k{}^2$ and $D\delta_{\sigma_k,0}$ belong to a bond connecting to site k, because these energies are shared among four nearest-neighbor bonds. The comparison

σ_i	σ_j	dilute $q=2$ Potts	BC
●	●	e^{K}	$e^{K_{\mathrm{BC}}-D_{\mathrm{BC}}/2}$
●	■	1	$e^{-K_{\mathrm{BC}}-D_{\mathrm{BC}}/2}$
●	○	$e^{D/4}$	$e^{-D_{\mathrm{BC}}/4}$
○	○	$e^{V+D/2}$	1

(48)

shows that the bond weights differ only by a constant factor when

$$K = 2K_{\mathrm{BC}}, \quad V = -K_{\mathrm{BC}}, \quad D = 4K_{\mathrm{BC}} + D_{\mathrm{BC}}, \tag{49}$$

for which both models thus become equivalent. We note that, although the Blume-Capel model Eq. (47) does not contain explicit vacancy-vacancy couplings, the resulting value of V is nonzero in general. Furthermore, the mapping of the $q=2$ dilute Potts model in the full three-dimensional parameter space (K,D,V) on a spin-1 Ising model requires the introduction of an additional parameter in the Blume-Capel model, such as in the Blume-Emery-Griffths model [33] which contains, in addition to Eq. (47), also a biquadratic coupling term proportional to $\Sigma s_i^2 s_j^2$. The Blume-Capel tricritical point is thus not the q=2 tricritical point as determined in Sec. III A, but arguments of universality predict it to have the same critical exponents. Exact critical exponents in this universality class are known from the mapping of the dilute Potts models with plaquette interactions on a Gaussian model [34] and, in an independent way, from the exact solution of the hard-square model [35,36].

We used the spin-1 representation to locate the tricritical point, because it enables us to perform transfer-matrix calculations up to finite size $L=16$, while these calculations based on Eq. (5) are restricted to $L\leqslant 12$. The solutions of Eqs. (22) (with K and D replaced by K_{BC} and D_{BC}) should, according to Eqs. (27) and (28), display finite-size dependences proportional to $L^{y_i-y_{t_1}}$ and $L^{y_i-y_{t_2}}$, i.e., $L^{-14/5}$ and $L^{-9/5}$ if we take $y_i=y_{t_3}=2-X_{1,4}=-1$. However, corrections proportional to $L^{-9/5}$ were not observed. Three-point fits (see Ref. [20]) to the solutions of Eqs. (22) yielded a correction exponent close to -2.81 with an uncertainty of about 10^{-2}. An explanation may be that the amplitudes a_t and u_t in Eq. (25) vanish, which is the case if the derivatives of the scaling function X_t to the temperaturelike fields t and u are zero.

We thus fixed the leading correction exponent as $-14/5$ in order to extrapolate the solutions of Eqs. (22). This leads to a sequence of iterated estimates that can again be subjected to iterated fits. These suggest that the leading finite-size dependence of the iterated fits is as $L^{-19/5}$ (where the exponent is equal to $2y_i-y_{t_1}$) or L^{-4}. The final estimates of K_f and D_f are based on iterated fits using the latter exponents, and on fits in which the finite-size exponents is left free. The numerical errors are estimated from the differences between these three types of fits, and on the differences between the results for subsequent finite sizes. We thus obtain the final estimates for the Blume-Capel tricritical point at $K_{\mathrm{BC}}=1.643\,175\,9(1)$, $D_{\mathrm{BC}}=3.230\,179\,7(2)$. These numbers are consistent with the literature values [37] $K_{\mathrm{BC}}=1.64(1)$, $K_{\mathrm{BC}}=3.22(2)$, and are sufficiently accurate for the Monte Carlo analyses mentioned in Sec. I. The finite-size results for the tricritical vacancy density were extrapolated by similar means as used in Sec. III A. This yielded $\rho=0.454\,950\,6(2)$.

We did not try to locate the critical fixed point of the Blume-Capel model because of the vanishing amplitude [7,27] of the irrelevant field. In view of the research of constrained systems, it is still desirable to obtain accurate numbers for the location of a critical point of a system subject to such a constraint. For this purpose we have located the Blume-Capel critical point at Ising coupling $K_{\mathrm{BC}}=1$ by solving for D_{BC} in the equation for the scaled magnetic correlation length as indicated in Eq. (15), using the Ising magnetic dimension $X_h=1/8$. The expected finite-size corrections have exponents equal to $y_1-y_{t_1}=-3$ and next negative integers -4, -5, and so on. We applied iterated fits as defined in Ref. [20], using a few of these exponents. To test the consistency of this procedure, we varied the procedure by varying the number of iteration steps and by leaving the exponent free in the last step. Our final estimate for the critical point at $K_{\mathrm{BC}}=1$ is $D_{\mathrm{BC}}=1.702\,717\,80(3)$.

B. Geometric tricritical fixed points for noninteger q

We study the fractal properties of percolation clusters constructed at the percolation threshold of tricritical Potts clusters. For integer q, this problem was already addressed in Ref. [15]. It was found that, when bonds are added with probability p between neighboring site variables in the same Potts state, the percolation threshold occurs at a value *smaller* than the random-cluster probability $p_{rc}=1-e^{-K}$. In contrast, the percolation threshold at Potts criticality lies precisely at p_{rc} [38]. This is natural because the so-called red-bond exponent [38], which governs the renormalization flow in the p-direction, is relevant on the Potts critical branch, but becomes irrelevant on the tricritical branch. On the tricritical branch, the random-cluster point thus no longer qualifies as a fixed point of this percolation problem. The renormalization flow at the random-cluster point is attracted by a stable fixed point at $p>p_{rc}$. A new unstable fixed point, called the geo-

metric fixed point, appears at $p<p_{rc}$, with critical exponents that are conjectured in Ref. [15], mainly on the basis of empirical evidence that the universality class of the geometric fixed point on the tricritical line corresponds with that of the random-cluster fixed point on the critical line with the same conformal anomaly, i.e., with the same value of the number m defined in Sec. I. These two fixed points therefore share the same exponents; the conjecture specifies the correspondence between the two sets, which we shall outline here for the magnetic dimensions X_h and the red-bond dimension X_p. To distinguish between the geometric and the random-cluster fixed points, we add superscripts g and r, respectively. For the random-cluster fixed point these dimensions are, as a function of g,

$$X_h^{(r)} = \frac{(g-2)(6-g)}{8g}, \quad X_p^{(r)} = \frac{(3g-4)(g+4)}{8g}, \tag{50}$$

where the expression for X_h is taken from Sec. I, and that for X_p was obtained [38] by means of Coulomb gas methods. Consider a Potts model on the critical branch with a coupling constant g and one on the tricritical branch with a coupling constant g'. From the relations between g and m listed in Sec. I, it follows that the two models are parametrized by the same number m when $gg'=16$. Therefore, the substitution of g by $16/g'$ in Eqs. (50) leads to some scaling dimensions on the other branch. The conjecture in Ref. [15] is that these are just the corresponding dimensions at the geometric fixed point. This conjecture supplements a second conjecture [15,39], in which the superscripts g and r are interchanged. Note that the partition sum does not depend on the percolation probability p, so that m must be independent of p. The substitution leads to

$$X_h^{(g)} = \frac{(8-g')(3g'-8)}{32g'}, \quad X_p^{(g)} = \frac{(12-g')(g'+4)}{8g'}. \tag{51}$$

Since Eq. (51) has only been tested for tricritical Potts models with an integer number of states, we investigate whether it also applies to Potts models with noninteger q.

In the absence of discrete Potts variables, we choose the random-cluster decomposition as a starting point, while preserving its bond variables. These have a probability p_{rc} between two Potts variables in the same state; one can thus form percolation clusters with a bond probability $p<p_{rc}$ by inserting a percolation bond with probability p/p_{rc} for each random-cluster bond that is present, and no percolation bond otherwise. These percolation bonds define a percolation problem that is, for $p<p_{rc}$, different from the random-cluster model. Naturally the investigation of this percolation problem still relies on the Monte Carlo simulation of the random-cluster model.

We performed such simulations, while constructing percolation clusters for a range of values of $p \leqslant p_{rc}$. We sampled the distribution of the cluster sizes and thus obtained the average squared cluster size

$$S^{(2)} = \left\langle \frac{1}{N^2} \sum_{i=1}^{n_c} c_i^2 \right\rangle \tag{52}$$

and the dimensionless ratio

$$Q = \frac{\langle \sum_{i=1}^{n_c} c_i^2 \rangle^2}{\langle 3(\sum_{i=1}^{n_c} c_i^2)^2 - 2\sum_{i=1}^{n_c} c_i^4 \rangle}, \tag{53}$$

where c_i is the size of the ith cluster, n_c the number of clusters, and N the number of total sites. Near the percolation threshold at $p=p_c$, the quantity Q scales as

$$Q = Q_0 + \sum_{k=1,2,\ldots} a_k (p-p_c)^k L^{k y_p^{(g)}} + \sum_{j=1,2,\ldots} b_j L^{y_j} + c(p-p_c) L^{y_p^{(g)}+y_1} + d(p-p_c)^2 L^{y_p^{(g)}} + \cdots, \tag{54}$$

and $S^{(2)}$ scales as

$$S^{(2)} = L^{-2X_h^{(g)}} \{ a_0 + a_1 (p-p_c) L^{y_p^{(g)}} + a_2 (p-p_c)^2 L^{2y_p^{(g)}} + \cdots + L^{y_1} [b_0 + b_1 (p-p_c) L^{y_p^{(g)}} + \cdots] \}, \tag{55}$$

where the $y_j (j=1,2,\ldots)$ are negative exponents describing corrections that will be discussed later, and the a_i, b_i, c, and d are unknown amplitudes.

TABLE V. Parameters describing the simulations of the tricritical Potts models. For each value of q we list the smallest and largest system sizes that were simulated, and the number n_L of system sizes in these ranges. We also show the range of p and the number n_p of points in this interval used for the simulations, and the number of samples n_s taken for the smallest and largest system sizes. The number of samples for all system sizes up to $L=84$ was equal to that for $L_{\min}$ in lines 2 and 3, and similar for those up to $L=96$ in line 4. For larger system sizes, the number of samples decreases gradually to that for $L_{\max}$, except for the system of the first line. The last column specifies the numbers of the Monte Carlo moves taken between subsequent samples. S stands for a site update, B for a bond update, FC for a full cluster decomposition, and M for a Metropolis sweep through the whole lattice.

q	$L_{\min}$	$L_{\max}$	n_L	Range of p	n_p	$n_s(L_{\min})$	$n_s(L_{\max})$	Update intervals
$2-\sqrt{2}$	4	36	11	0.56–0.61	6	1×10^8	1×10^8	$L^2/5$ S+$L^2/3$ B
$2-\sqrt{2-\sqrt{2}}$	4	160	17	0.58–0.60	5	6×10^7	4×10^6	$L/5$ (FC+M)
$2+\sqrt{2-\sqrt{2}}$	4	200	20	0.61–0.645	8	12×10^7	7×10^6	$L/5$ (FC+M)
$2+\sqrt{2}$	4	160	17	0.63–0.68	6	1×10^8	8×10^6	$L/5$ (FC+M)

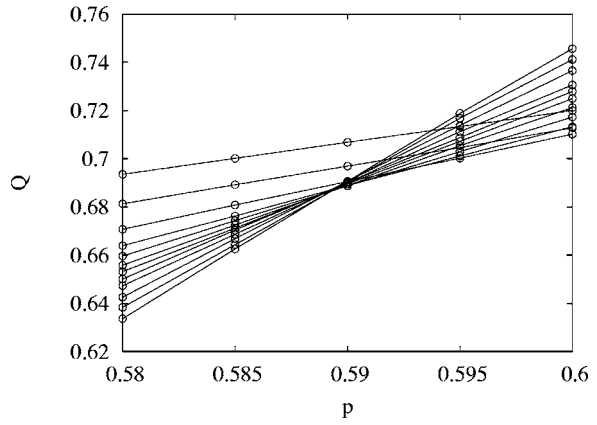

FIG. 4. Determination of the geometric fixed point of the tricritical $(2-\sqrt{2-\sqrt{2}}=1.234\ldots)$-state dilute Potts model. The date shown apply to 12 system sizes in the range $6 \leqslant L \leqslant 84$. The lines connect data points with the same L. Their slopes increase with L, and their intersections reveal the location of the unstable fixed point, i.e., the percolation threshold. The error bars of the data points do not exceed the line thickness.

The ratio Q is a useful quantity to locate phase transitions and to determine the associated temperaturelike exponent. From Eq. (54) one finds that the Q versus p curves for different values of L tend to intersect at values approaching $p=p_c$ for large L. Moreover, the slopes of these curves behave as $L^{y_p^{(g)}}$ which allows the estimation of $y_p^{(g)}$.

The simulations took place for four values of q, viz., $q=2\pm\sqrt{2}$ and $q=2\pm\sqrt{2-\sqrt{2}}$. The number of vacancies was conserved as described in Sec. II B. Since the number of vacancies in a simulation is restricted to an integer, the result for a given density was obtained by a weighted averaging over two simulations with a different number of vacancies. The simulations for $q=2-\sqrt{2}$ used local updates and were more time consuming than those for the other values of q, and thus restricted to relatively small system sizes. The data for the system sizes, simulation lengths, and intervals of p are summarized in Table V.

The results for the dimensionless ratio Q are shown in Fig. 4 for the case $q=2-\sqrt{2-\sqrt{2}}$. The intersections reveal the location of the geometric fixed point. A more accurate location was determined by a least-squares analysis according to Eq. (54). Similar analyses were performed for the other three values of q. These fits included up to three coefficients a_k, and three or four coefficients b_j, depending on the χ^2 criterion. The corresponding correction exponents y_j were fixed equal to the third temperature exponent, twice this number, and/or equal to the negative integers -1, -2, -3, etc., such that largest (closest to 0) exponents appear first. In order to reduce the residual χ^2 to acceptable values, the smallest system sizes $L<6$ had to be discarded for all four values of q. Furthermore, we have fitted an expression of the form Eq. (55) to the simulation data for $S^{(2)}$ which is, except for a factor L^2, a susceptibilitylike quantity, using a similar set of finite-size corrections as for Q. These fits allow the determination of $X_h^{(g)}$. The numerical results for the exponents, which are included in Table VI, are in good agreement with the exact values predicted by Eqs. (51).

VI. CONCLUSION

In line with previous work [40] we observe that finite-size scaling analysis based on transfer-matrix calculations provides an efficient tool for the analysis of critical phenomena and the determination of phase diagrams of two dimensional models, even though the accessible range of finite sizes is quite limited. This limitation is compensated by the high numerical accuracy of the transfer-matrix results for the eigenvalues, which allow the application of iterated fitting procedures, especially when the scaling dimensions are known from other sources. The latter point is relevant for an evaluation of the present transfer-matrix analysis of the dilute Potts model. Two points of view are possible. First, one may focus on the question whether the renormalization description of Nienhuis *et al.* [1], and the exact results for the exponents based on arguments of universality, are applicable to the present model described by Eq. (1). While this seems plausible, rigorous evidence is not available so that numerical tests are justified. Our analysis does indeed provide ample numerical evidence. We note that, if the expressions for the scaling dimensions X_h and X_t listed in Sec. I were

TABLE VI. Geometric fixed points of several tricritical Potts models with a noninteger number of states q. The numerical values of the percolation threshold p_c, the red-bond exponent $y_p^{(g)}$, and the magnetic dimension $X_h^{(g)}$ at the geometric fixed point are obtained by fitting formulas given in the text to the simulation data. The table also lists the conjectured exact values of $y_p^{(g)}$ and $X_h^{(g)}$ (see text). The results for p_c are listed as p_{c_i} where $i=1$, 2 refer to different fits: p_{c_1} and $y_p^{(g)}$ are obtained from fits to the ratio Q in which $y_p^{(g)}$ appears as a free parameter, and p_{c_2} is obtained with $y_p^{(g)}$ fixed at its conjectured value. The magnetic exponent $X_h^{(g)}$ is obtained by a fit to the average squared cluster size with $y_p^{(g)}$ fixed at the conjectured value, and p_c fixed at p_{c_2}. Fits that leave p_c as a free parameter lead to consistent results but with slightly larger error bars.

q	g	$y_p^{(g)}$	$y_p^{(g)}$ (exact)	$X_h^{(g)}$	$X_h^{(g)}$ (exact)	p_{c_1}	p_{c_2}
$2-\sqrt{2}$	11/2	0.59 (4)	105/176	0.12 (1)	85/704	0.581 (5)	0.581 (4)
$2-\sqrt{2-\sqrt{2}}$	21/4	0.511 (8)	115/224	0.125(2)	341/2688	0.5906(5)	0.5906(4)
$2+\sqrt{2-\sqrt{2}}$	19/4	0.334(10)	201/608	0.135(3)	325/2432	0.6300(5)	0.6300(4)
$2+\sqrt{2}$	9/2	0.225 (8)	11/48	0.136(5)	77/576	0.6604(6)	0.6601(4)

TABLE VII. Numerical results for the conformal anomaly of the dilute Potts model, for several points on the critical and tricritical branches. Comparison with the exact results (also listed) confirms that the present models fit well within the known Potts universality classes.

q	g	m	c (numerical)	c (exact)
2.45	3.1444…	3.6754…	0.6509(1)	0.650854…
$2+\sqrt{2-\sqrt{3}}$	19/6	19/5	0.6711(1)	51/76
2.8	3.2619…	4.4199…	0.7496(1)	0.749535…
3	8/3	6	0.8000(1)	4/5
3.5	3.5398…	7.6936…	0.9103(1)	0.910294…
3.9	3.7978…	18.7857…	0.9839(1)	0.983857…
4	14/3	∞	1.0000(1)	1
3.9	4.2021…	19.7857…	0.9855(1)	0.985410…
3.5	4.4601…	8.6936…	0.9288(1)	0.928802…
$2+\sqrt{2}$	9/2	8	0.9167(1)	11/12
3	14/3	6	0.8571(1)	6/7
$2+\sqrt{2-\sqrt{2}}$	19/4	16/3	0.8224(1)	0.822368…
2.5	4.8391…	4.7667…	0.7817(1)	0.781731…
2	5	4	0.7000(1)	7/10
1.5	5.1608…	3.4457…	0.6083(1)	0.608321…
$2-\sqrt{2-\sqrt{2}}$	21/4	16/5	0.5537(2)	0.553571…
1	16/3	3	0.5000(1)	1/2
$2-\sqrt{2}$	11/2	8/3	0.3858(5)	17/44
$2-\sqrt{3}$	17/3	12/5	0.262 (4)	9/34
0.1	5.7978…	2.2248…	0.160 (5)	0.163771…

incorrect, that this would be revealed in the fitting procedures for the fixed points by corrections decaying slower than expected, as mentioned in Sec. III A, unless the differences with the true exponents would accidentally be very small. Furthermore, also the consistency of the results for the conformal anomaly, listed in Table VII, with the existing theory supports the assumptions made. Our results for c supplement those already given in Ref. [28], in particular most results for the tricritical branch are new. Here we add the comment that the format of Ref. [28] precluded a discussion of the numerical errors. In one case, this led to a somewhat misleading result, namely the entry for the $q=4$ Potts model without vacancies in Table II of Ref. [28]. The finite-size data for the conformal anomaly are poorly convergent because of logarithmic corrections induced by the second temperature field which is marginal at $q=4$. However, the fit applied to those finite-size data produced an erratic numerical result that was much closer to the theoretical value of c than what one could have expected in view of the actual numerical accuracy. Therefore the agreement for $q=4$ looked better than it actually was. The present analysis of c at the estimated fixed point does not noticeably suffer from such numerical problems, and does indeed produce a result (see Table VII) very close to the expected value $c=1$. As another confirmation, the results for the fixed line and for the phase diagram of the $q=2-\sqrt{2}$ model, are in a complete qualitative agreement with the results presented in Ref. [1]. We also note that this applies as well to the renormalization analysis of the Blume-Emery-Griffiths model [33], which was worked out in considerable detail by Berker and Wortis [41].

As a second point of view, one may accept the Potts renormalization scenario and the literature values of the scaling dimensions as true for the present model, and thus interpret our results in terms of relatively accurate information on the phase diagram and the location of what serves effectively as a line of fixed points in the phase diagram in the (q,K,D) parameter space, including a line of tricritical transitions. These results are well applicable in Monte Carlo investigations of tricritical Potts models and $q\approx 4$ Potts models, including numerical analysis of the Fisher renormalization phenomenon. Preliminary results have already been used [11,14,15]. Minor differences with respect to the values quoted in the present work appear because data for larger system sizes are included here.

ACKNOWLEDGMENTS

We thank Jouke Heringa and Bernard Nienhuis for valuable discussions. This research is supported by the Dutch FOM foundation ("Stichting voor Fundamenteel Onderzoek der Materie") which is financially supported by the NWO ("Nederlandse Organisatie voor Wetenschappelijk Onderzoek").

APPENDIX A: CODING THE CONNECTIVITIES

The construction of the transfer matrix requires a "coding" of the relevant degrees of freedom at the open end of the cylinder, by means of integers 1, 2, … that will serve as a transfer-matrix index. This code specifies which sites of the nth layer are vacant, and how the remaining sites are mutually connected by some path of bonds in rows 1 to n. Since we are interested in the magnetic correlation function, which in the language of the random-cluster model is the probability that two sites belong to the same cluster, we use connectivities of the magnetic type which, in addition, specifies which sites of row n are still connected to a site in row 1. These connectivities satisfy a "well-nestedness" property which says that the sites labeled $1,2,\ldots,L$ on row n obey the following rule: if site i is connected to site k, and site j is connected to site l while $i<j<k<l$, all four sites must be connected. Since a complete definition of the coding of the general connectivities is somewhat elaborate, we make use of some definitions already given in Ref. [20]. There, an L-point connectivity is represented by a row of L integers $i_1,i_2,\ldots,i_L$, such that connected sites are represented by equal integers, and by different integers if they are not connected. A subset of sites connected to a "ghost site" (which are not necessarily well nested) were represented by the special integer 0. These connectivities were coded by an integer $\tau(i_1,i_2,\ldots,i_L)$ defined in Ref. [20]. Since one can alternatively interpret the zeros in the row $i_1,i_2,\ldots,i_L$ as vacancies, it follows that the same coding $\tau(i_1,i_2,\ldots,i_L)$ applies to nonmagnetic connectivities with vacancies. The number of such connectivities on L sites is denoted d_L, also given in Ref. [20]. Here we consider the more general problem of coding the connectivities with well-nested magnetic sites (labeled by

-1) as well as vacancies (labeled by 0). First, we code the positions of the magnetic sites by means of a binary number $m=0,1,\ldots,2^L-1$, where the binary digit 1 denotes a magnetic site. The magnetic sites divide the remaining sites in $g(m)$ groups such that two sites in different groups are not connected because of the well-nestedness property. Let there be $t(m,j)$ sites in the jth group. There are thus

$$h_m \equiv d_{t(m,1)} d_{t(m,2)} \cdots d_{t(m,g(m))} \tag{A1}$$

connectivities with magnetic subcode m, and the total number of general connectivities is

$$G_L = \sum_{m=0}^{2^L-1} h_m. \tag{A2}$$

To assign a unique integer to each of these connectivities, we need to specify an "ordering" of the connectivities. In addition to the ordering defined in Ref. [20], we order the magnetic subcode according to the value of m. Thus a general connectivity $i_1, i_2, \ldots, i_L$ with magnetic subcode $m(i_1, i_2, \ldots, i_L)$ is coded by the integer

$$\gamma(i_1, i_2, \ldots, i_L) \equiv 1 + \sum_{k=0}^{m-1} h_k + \sum_{l=1}^{g(m)} (\tau_l - 1) \prod_{j=2}^{l} d_j, \tag{A3}$$

where τ_l is the code (using the definition in Ref. [20]) for the lth group of nonmagnetic sites. A decoding algorithm was constructed on the basis of essentially the same ideas.

APPENDIX B: CONSTRUCTION OF THE TRANSFER MATRIX

Consider a system on a cylinder with a length of n circular rows. We denote the variables in row j, bond as well as site variables, by $\vec{s}_j$. Its partition sum is written in the form

$$Z^{(n)} = \sum_{\vec{s}_1,\ldots,\vec{s}_n} W_n(\vec{s}_1, \vec{s}_2, \ldots, \vec{s}_n) \tag{B1}$$

with $W_n(\vec{s}_1, \vec{s}_2, \ldots, \vec{s}_n) \equiv \exp[-\mathcal{H}_n(\vec{s}_1, \vec{s}_2, \ldots, \vec{s}_n)/kT]$ which denotes the Boltzmann factor of the given configuration of variables, including the weights of all bonds, sites, and components. Let κ_n be the connectivity on row n. It is, in principle, a function of all the variables $\vec{s}_j$, $j=1,2,\ldots,n$. We divide $Z^{(n)}$ into contributions for different values of κ_n:

$$Z_\alpha^{(n)} = \sum_{\vec{s}_1,\ldots,\vec{s}_n} \delta_{\alpha,\kappa_n(\vec{s}_1,\ldots,\vec{s}_n)} W_n(\vec{s}_1, \vec{s}_2, \ldots, \vec{s}_n) \tag{B2}$$

with

$$Z^{(n)} = \sum_{\alpha=1}^{G_L} Z_\alpha^{(n)}. \tag{B3}$$

Similarly we have

$$Z_\alpha^{(n+1)} = \sum_{\vec{s}_1,\ldots,\vec{s}_{n+1}} \delta_{\alpha,\kappa_{n+1}(\vec{s}_1,\ldots,\vec{s}_{n+1})} W_{n+1}(\vec{s}_1, \vec{s}_2, \ldots, \vec{s}_{n+1}). \tag{B4}$$

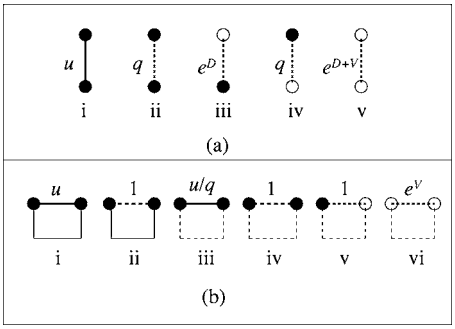

FIG. 5. Weights of the vertical and horizontal bonds as they appear in the sparse-transfer-matrix technique. New sites are appended in the upper row, which thus also accounts for the site weights q and e^D.

Here we may substitute

$$W_{n+1} = W_n w(\kappa_n, \vec{s}_{n+1}), \tag{B5}$$

where w denotes the weight of the newly appended row, which accounts for the weights of the site variables and the bond variables, and the change in the number of components. Furthermore we can substitute

$$\kappa_{n+1} = \mu(\kappa_n, \vec{s}_{n+1}), \tag{B6}$$

which expresses that the connectivity on row $n+1$ depends only on that on row n and on the variables in the appended row. Thus

$$Z_\alpha^{(n+1)} = \sum_{\vec{s}_1,\ldots,\vec{s}_{n+1}} \delta_{\alpha,\mu(\kappa_n,\vec{s}_{n+1})} W_n(\vec{s}_1, \ldots, \vec{s}_n) w(\kappa_n, \vec{s}_{n+1}). \tag{B7}$$

We may insert a factor $\Sigma_{\beta=1}^{G_L} \delta_{\beta,\kappa_n(\vec{s}_1,\ldots,\vec{s}_n)} = 1$ which leads to

$$Z_\alpha^{(n+1)} = \sum_{\beta=1}^{G_L} \sum_{\vec{s}_1,\ldots,\vec{s}_n} \delta_{\beta,\kappa_n(\vec{s}_1,\ldots,\vec{s}_n)} W_n(\vec{s}_1, \vec{s}_2, \ldots, \vec{s}_n) \times \sum_{\vec{s}_{n+1}} \delta_{\alpha,\mu(\beta,\vec{s}_{n+1})} w(\beta, \vec{s}_{n+1}). \tag{B8}$$

The middle part of this expression is $Z_\beta^{(n)}$, and the last part is the transfer matrix

$$T_{\alpha\beta} \equiv \sum_{\vec{s}} \delta_{\alpha,\mu(\beta,\vec{s})} w(\beta, \vec{s}), \tag{B9}$$

so that we may write the recursion for the restricted partition sum as

$$Z_\alpha^{(n+1)} = \sum_\beta T_{\alpha\beta} Z_\beta^{(n)}. \tag{B10}$$

The algorithm that performs a multiplication of a vector by the transfer matrix forms the main ingredient for the calculation of a few of the leading eigenvalues of $T_{\alpha\beta}$.

To enable calculations for system as large as possible, the transfer matrix is decomposed into $2L$ sparse matrices, each of which accounts for one bond variable, while L of these also account for appending a new site variable. This sparse-matrix decomposition leads to a very significant reduction of

the required computer time and memory. The decomposition is the same as for the nearest-neighbor Potts model without vacancies, which was described in Ref. [20]. The weights associated with the vertical bonds (which include those of the new sites appended to the cylinder) and the horizontal bonds (which may close a loop, so that their weights depend on whether or not the sites are already connected) are given in Fig. 5. These sparse matrices are defined such that they do not only account for the weight of a particular bond, they also permute the vertices in such way that only two different sparse matrices remain, one for the vertical bonds and one for the horizontal ones.

[1] B. Nienhuis, A. N. Berker, E. K. Riedel, and M. Schick, Phys. Rev. Lett. **43**, 737 (1979).
[2] R. J. Baxter, J. Phys. C **6**, L445 (1973).
[3] M. Nauenberg and D. J. Scalapino, Phys. Rev. Lett. **44**, 837 (1980).
[4] J. L. Cardy, M. Nauenberg, and D. J. Scalapino, Phys. Rev. B **22**, 2560 (1980).
[5] J. Salas and A. D. Sokal, J. Stat. Phys. **88**, 567 (1997).
[6] P. W. Kasteleyn and C. M. Fortuin, J. Phys. Soc. Jpn. **26**, 11 (1969); C. M. Fortuin and P. W. Kasteleyn, Physica (Amsterdam) **57**, 536 (1972).
[7] B. Nienhuis, in *Phase Transitions and Critical Phenomena*, edited by C. Domb and J. L. Lebowitz (Academic, New York, 1987), Vol. 11.
[8] J. L. Cardy, in *Phase Transitions and Critical Phenomena*, edited by C. Domb and J. L. Lebowitz (Academic, New York 1987), Vol. 11.
[9] P. Grassberger, J. Phys. A **25**, 5475 (1992).
[10] P. Grassberger, Physica A **262**, 251 (1999).
[11] Y. Deng, H. W. J. Blöte, and B. Nienhuis, Phys. Rev. E **69**, 026114 (2004).
[12] L. Chim, Int. J. Mod. Phys. A **11**, 4491 (1996).
[13] I. Affleck, J. Phys. A **33**, 6473 (2000).
[14] Y. Deng and H. W. J. Blöte, Phys. Rev. E **70**, 035107(R) (2004).
[15] Y. Deng, H. W. J. Blöte, and B. Nienhuis, Phys. Rev. E **69**, 026123 (2004).
[16] B. Nienhuis, Physica A **177**, 109 (1991).
[17] M. E. Fisher, Phys. Rev. **176**, 257 (1968).
[18] J. R. Heringa and H. W. J. Blöte, Physica A **232**, 369 (1996); Phys. Rev. E **57**, 4976 (1998).
[19] M. P. Nightingale, Phys. Lett. **59**, 486 (1977); Proc. K. Ned. Akad. Wet., Ser. B: Phys. Sci. **82**, 235 (1979).
[20] H. W. J. Blöte and M. P. Nightingale, Physica A **112**, 405 (1982); in *Finite-Size Scaling*, edited by J. L. Cardy (North Holland, Amsterdam, 1988).
[21] J. L. Cardy, J. Phys. A **17**, L358 (1984).
[22] M. Sweeny, Phys. Rev. B **27**, 4445 (1983).
[23] F. Gliozzi, Phys. Rev. E **66**, 016115 (2002).
[24] L. Chayes and J. Machta, Physica A **254**, 477 (1998).
[25] X. Qian, Y. Deng, and H. W. J. Blöte, Phys. Rev. E **71**, 016709 (2005).
[26] X. Qian, Y. Deng, and H. W. J. Blöte, Phys. Rev. B **71**, 144303 (2005).
[27] H. W. J. Blöte and M. P. M. den Nijs, Phys. Rev. B **37**, 1766 (1988).
[28] H. W. J. Blöte, J. L. Cardy, and M. P. Nightingale, Phys. Rev. Lett. **56**, 742 (1986).
[29] I. Affleck, Phys. Rev. Lett. **56**, 746 (1986).
[30] D. Friedan, Z. Qiu, and S. Shenker, Phys. Rev. Lett. **52**, 1575 (1984).
[31] R. B. Potts, Proc. Cambridge Philos. Soc. **48**, 106 (1952).
[32] M. Blume, Phys. Rev. **141**, 517 (1966); H. W. Capel, Physica (Amsterdam) **32**, 966 (1966).
[33] M. Blume, V. J. Emery, and R. B. Griffiths, Phys. Rev. A **4**, 1071 (1971).
[34] B. Nienhuis, J. Phys. A **15**, 199 (1982).
[35] R. J. Baxter, J. Stat. Phys. **26**, 427 (1981).
[36] D. A. Huse, Phys. Rev. Lett. **49**, 1121 (1982).
[37] P. D. Beale, Phys. Rev. B **33**, 1717 (1986).
[38] A. Coniglio and W. Klein, J. Phys. A **13**, 2775 (1980); A. Coniglio, Phys. Rev. Lett. **62**, 3054 (1989).
[39] W. Janke and A. M. J. Schakel, Nucl. Phys. B **700**, 385 (2004).
[40] For reviews, see, e.g., M. P. Nightingale, in *Finite-Size Scaling and Numerical Simulation of Statistical Systems* edited by V. Privman (World Scientific, Singapore, 1990); and M. N. Barber, in *Phase Transitions and Critical Phenomena*, edited by C. Domb and J. L. Lebowitz (Academic, New York, 1983), Vol. 8.
[41] A. N. Berker and M. Wortis, Phys. Rev. B **14**, 4946 (1976), and references therein.